ACS OMEGA

http://pubs.acs.org/journal/acsodf
Article

Large-Size and Ultrahigh Purity Tungsten with Enhanced Physical Properties via Chemical Vapor Deposition

Lipei Peng, Shiwei Wu, Xicheng Wei, Wei Peng, Yafeng Wang, Tengshi Liu, Shaobo Li, Xiangjun Meng,* and Han Dong*

Cite This: *ACS Omega* 2024, 9, 42549−42556

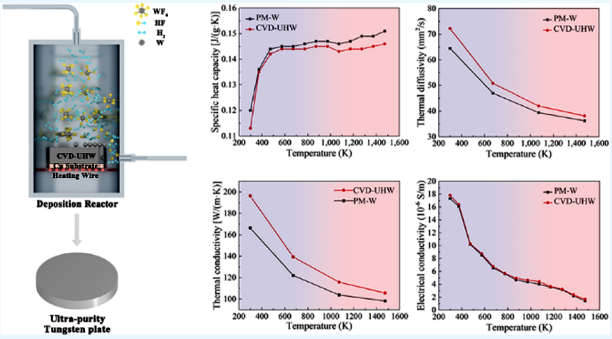

ABSTRACT: Conventional powder metallurgy techniques fail to meet the demands for ultrahigh purity tungsten (UHPW) and scalable component sizes required by the semiconductor industry. In this study, ultrahigh purity (99.999998 wt %) large-size tungsten parts, with an adjustable thickness and a diameter of 350 mm, were prepared via a chemical vapor deposition (CVD) method using ultrahigh purity (99.9999 wt %) tungsten hexafluoride (WF_6) as the precursor. The microstructure and physical properties of the resulting CVD-UHPW were evaluated and compared with those of powder metallurgy tungsten (PM-W). The results indicate that CVD-UHPW displays a columnar grain microstructure with a lower dislocation density and internal strain, whereas PM-W shows an equiaxed grain microstructure. CVD-UHPW has a density of 19.17 g/cm^3, closely matching the theoretical density of tungsten (19.35 g/cm^3) and significantly higher than PM-W's density of 18.79 g/cm^3. The specific heat capacities of CVD-UHPW, measured from 298 to 1473 K, range from 0.113 to 0.146 J/g·K, similar to PM-W's range of 0.120 to 0.151 J/g·K. CVD-UHPW shows improved electrical and thermal conductivities compared to PM-W, with values ranging from 1.68×10^6 to 1.78×10^7 S/m and 105.7 to 196.4 W/(m·K) from 298 to 1473 K. This study highlights the potential of the CVD method for the large-scale production of ultrahigh purity tungsten parts, emphasizing its significant applicability across various industries.

1. INTRODUCTION

Tungsten (W) materials have found widespread applications across various advanced fields of electronics,[1] nuclear energy,[2−5] medicine,[6] and aerospace,[7] because of their unique properties including high melting point, density, hardness, low vapor pressure, low thermal expansion coefficient, and excellent radiation shielding and thermal conductivity.[8,9] Particularly in microelectronics, tungsten is widely used as a sputtering target in the manufacturing of very large scale integrated circuits (VLSI), thanks to its stability and excellent conductivity. It is utilized in the production of critical components in semiconductors such as diffusion barriers, vias, and gate materials. However, these applications require tungsten materials to achieve ultrahigh purity with controlled properties, like density, grain size, and orientation, to ensure optimal performance of thin films.[10−12] On the other hand, tungsten metals and alloys are used in various forms with different size requirements, including coatings,[13] films,[14] and parts[15] such as plates, wires, tubes, and crucibles. Therefore, developing efficient methods and processes to produce highly pure, dense, and specifically shaped tungsten materials of various sizes has been a long-standing research focus.

Hitherto, many application-specific methods have been developed for tungsten production, with the most commonly used being powder metallurgy (PM)[16−18] and chemical vapor deposition (CVD).[19−22] Despite the widespread use of PM and CVD technologies in tungsten production, significant challenges remain in achieving high purity and large-scale production simultaneously. The PM method allows for high production capacities and is suitable for large-scale manufacturing. However, its multistep process nature is apt to introduce various difficult-to-remove metallic impurities, limiting the product purity to between 99.5% and 99.9%.[23,24] It is generally accepted[25−31] that to achieve fully dense, high-purity, and large-sized tungsten coatings of various shapes, the CVD method is superior to PM and other coating methods like vacuum plasma spraying (VPS) and physical vapor deposition

Received: July 21, 2024
Revised: August 20, 2024
Accepted: September 26, 2024
Published: October 4, 2024

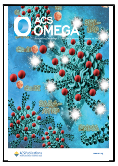

https://doi.org/10.1021/acsomega.4c06723

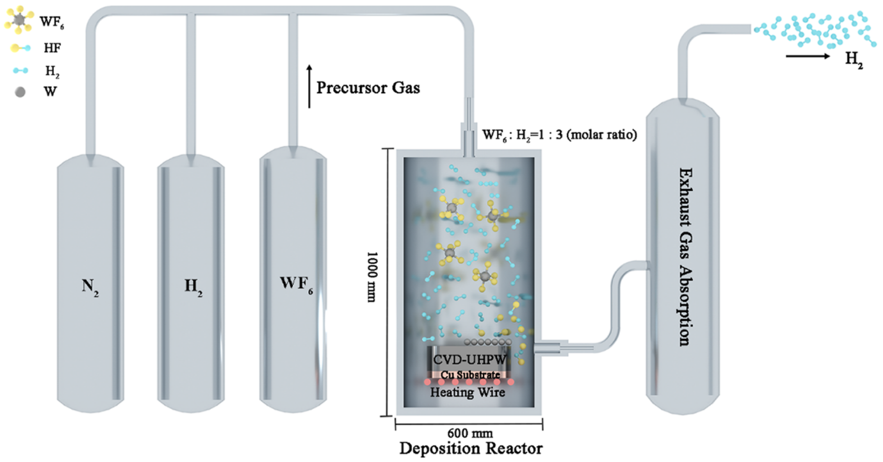

Figure 1. Schematic of the deposition system for CVD-UHPW.

(PVD). In the CVD method, precursor gases undergo heterogeneous gas-to-solid surface reactions on specific substrates, allowing for precisely controlled compositions and purities. The CVD method for tungsten coatings dates to 1959 and has been extensively studied since then. A well-established process uses tungsten hexafluoride as the precursor and hydrogen as the reducing agent. Along this line of CVD chemistry, Ma et al.[19−22] prepared various products such as tungsten tubes of different diameters and highly dense tungsten products. However, the tungsten materials aforementioned in those previous studies were all produced at laboratory scales and did not meet the size requirements for semiconductor targets. Kim et al.[29] determined the purity of their fabricated CVD-W plates by measuring the impurity contents of 14 elements, showing a purity of 99.99999 wt %. In a relatively recent work by Lv et al.,[31] large-size CVD-W parts, i.e., coating parts and shell parts, were prepared with a purity of 99.999978 wt %, showing excellent thermal properties compared to a PM-W sample. Although previous works have successfully prepared highly pure and shaped tungsten parts, there is still a need to develop more effective CVD methods to produce ultrahigh purity (surpassing 99.99999 wt %) tungsten parts on a large scale with comprehensive impurity measurements. This will meet the stringent purity criteria of VLSI manufacturers and provide a better understanding of their physical and functional properties.

This study focuses on the fabrication of ultrahigh purity tungsten (UHPW) with a purity exceeding 99.99999 wt % and sizes over hundreds of millimeters using the CVD technique, with a particular focus on its usage as sputtering targets in manufacturing VLSI. To achieve this, we describe the experimental setup and procedures for the CVD reactor system used to produce UHPW. We perform a comparative analysis of CVD-UHPW and PM-W in terms of purity, phase structure, microstructure, and functional properties. We demonstrate a practical application of the UHPW material and summarize the key findings from the analyses and discussions. Moreover, it is hoped that this study opens up new possibilities for the application of CVD-derived UHPW materials in high-tech industries, including advanced electronics, nuclear energy, and aerospace.

2. EXPERIMENTAL SECTION

The fabrication of CVD-UHPW was carried out in a system comprising a gas supply unit, a deposition reactor, a heating system, and an exhaust gas absorption column, as shown in Figure 1. The gas feed line delivered a vaporous mixture of highly pure WF_6 and H_2 in a 1:3 molar ratio. WF_6, with a purity of 99.9999 wt %, was supplied by PERIC Special Gases Co., Ltd., and H_2, with a purity of 99.999 wt %, was purchased from Air Products and Chemicals, Inc. The deposition reactor is a custom-built cold wall, vertical flow CVD reactor operating at atmospheric pressure, similar to the design detailed elsewhere.[32] A copper substrate with a diameter of 350 mm was positioned coaxially near the bottom of the reactor. During deposition, the substrate temperature was maintained at 843 K by the heating system depending on the operational conditions. The exhaust gas was absorbed using a calcium hydroxide-saturated solution in an adsorption column.

The system was designed with an average deposition rate of 0.2 mm/h and a production capacity of up to 10 tons per year. For illustration, the synthesized disk-shaped sample with a diameter of 350 mm and a thickness of 10 mm, which was separated from the copper substrate, is shown in Figure 2a. To identify the crystal phase structures, X-ray diffraction (XRD, Smartlab XRD) analysis was performed on the CVD-UHPW sample. For comparison, a commercial PM-W component measuring 10 × 10 × 10 mm^3 was also analyzed using the same method. Figure 2b shows that the XRD patterns of the two samples exhibit sharp peaks at 40.26°, 58.27°, 73.20°, and 87.02°, corresponding to the (110), (200), (211), and (220)

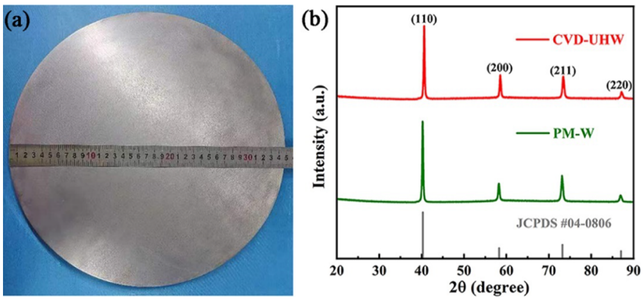

Figure 2. (a) Photo of the synthesized CVD-UHPW plate. (b) XRD patterns of CVD-UHPW and PM-W.

planes of single-phase cubic tungsten (JCPDS No. 04-0806). The similarity in the XRD patterns of the two samples indicates their preferential growth in the direction of the (100) plane.

For further characterization of both CVD-UHPW and PM-W samples, glow discharge mass spectrometry (GD-MS, Element GD Plus) was used to analyze trace impurities with a detection limit of 0.005 ppm. The remaining C, H, O, and N were analyzed by using instrumental gas analysis (IGA, LECO). Density measurements were performed by using an electronic balance (DS-100E) with a precision of 0.01 g/cm^3. The microstructures of both samples were analyzed using a scanning electron microscope (SEM, Apreo2S), an electron backscatter diffraction (EBSD) instrument (Bruker e-flash2), and a transmission electron microscope (TEM, FEI Tecnai G2 F20). Thermal diffusivity was measured by using the laser flash method (LFA467 Hyper Flash). Specific heat capacity was measured by using a synchronous thermal analyzer (STA449F3). Thermal conductivity was calculated using the equation $k = \alpha \times \rho \times C_p$, where k represents thermal conductivity, α is the thermal diffusivity, ρ is the density, and C_p is the specific heat capacity. Electrical conductivity was measured using a conductivity meter (SBA458).

3. RESULTS AND DISCUSSION

In the first place, a comprehensive measurement of trace impurities, covering 68 elements in both samples, was conducted. The results, shown in Table 1, reveal that the purity of CVD-UHPW is 99.999998 wt %, while the purity of PM-W is 99.99921 wt %, significantly lower than that of CVD-UHPW. A scrutiny of certain impurities, including Ba, Cr, Fe, and Mo, in the table shows that their contents in the PM-W exceed 0.5 ppm, giving rise to the lower purity. In the work by Kim et al.,[29] the purity level of the CVD-W plates is attributed to quite low metallic impurity levels, while the purity of CVD-W reported[31] is as high as 99.999978 wt % but still less than that of the present CVD-UHPW due to its higher impurity contents of metal elements such as Al, Ca, Ti, Cr, Fe, Ni, and Zn. These impurity analysis results suggest a direct connection between tungsten purity and the feed reactants. In this study, the use of ultrahigh purity gaseous WF_6 (99.9999 wt %) ensures a clean reactive atmosphere during deposition. Besides, the residue element F in the CVD-UHPW is maintained at a low level, i.e., <0.05 ppm. Considering the possible incorporation of fluorine due to precursor WF_6 and/or product HF, the effective exclusion of F from CVD-UHPW in the present process is remarkable.

The measured contents of four nonmetallic impurities of concern in the application are listed in Table 2 for the two samples. It is seen that in both samples, residue levels of C, H, O, and N are well below the detection limits of the instrument used. Among the four elements, the residue O is known to significantly affect the sputtering rates of tungsten targets and the resulting film quality.[33] In the CVD-W reported by Kim et al.,[29] the O content was 3.2 ppm, and in the CVD-W by Lv et al.,[31] the O content was 7 ppm. Compared to these, the residue level of O in the present work is effectively controlled by using the precursor WF_6 with a purity of 99.9999 wt %.

Densities of the two types of tungsten were measured at 298 K on five samples, respectively. The average density of CVD-UHPW is 19.17 g/cm^3, which is close to the theoretical density of pure tungsten, namely 19.35 g/cm^3, and is 2% higher than the 18.79 g/cm^3 of PM-W. In the literature, great efforts have been made to prepare highly dense tungsten materials for various purposes. Therefore, an extended comparison was made using density vs component volume data from different studies employing various methods, including electron beam melting (EBM),[34,35] wire and arc additive manufacturing (WAAM),[36] CVD,[31,37] laser bed fusion (LBF),[38] PM,[39] and laser melting (LM).[40−43] Figure 3 shows that CVD-UHPW is located at the upper right corner, indicating that it achieves both high density (ultrahigh purity) and large volume. This suggests that the current CVD-UHPW has an advantageous combination of density (purity) and scalable size compared to those of many other methods.

Table 1. Metal Impurity Contents in Different Tungsten Samples

Element	CVD-UHPW/ppm	PM-W/ppm	Element	CVD-UHPW/ppm	PM-W/ppm
Li	<0.005	<0.005	Ag	<0.01	<0.01
Be	<0.001	<0.005	Cd	<0.01	<0.01
B	<0.001	<0.005	In	<0.01	<0.05
F	<0.05	<0.01	Sn	<0.01	0.01
Na	<0.005	<0.005	Pd	<0.01	<0.01
Mg	<0.005	<0.005	Te	<0.01	<0.01
Al	<0.005	0.06	I	<0.01	<0.01
Si	<0.005	0.04	Cs	<0.01	<0.01
P	<0.01	0.06	Ba	<0.005	0.78
S	0.02	0.02	La	<0.005	<0.005
K	<0.01	0.07	Pr	<0.005	<0.005
Ca	<0.01	0.06	Nd	<0.005	<0.005
Sc	<0.001	<0.001	Sm	<0.005	<0.005
Ti	<0.001	0.007	Eu	<0.005	<0.005
V	<0.001	0.004	Gd	<0.005	<0.005
Cr	<0.005	1.3	Tb	<0.005	<0.005
Mn	<0.001	0.05	Dy	<0.005	<0.005
Fe	<0.005	1.7	Ho	<0.005	<0.005
Co	<0.001	0.006	Er	<0.005	<0.005
Ni	<0.005	0.36	Tm	<0.005	<0.005
Cu	<0.01	0.08	Yb	<0.005	<0.005
Zn	<0.01	<0.01	Lu	<0.005	<0.005
Ga	<0.01	<0.01	Hf	<0.005	<0.005
Ge	<0.01	<0.01	Ta	<5	<1
As	<0.01	<0.01	Re	<0.05	<0.05
Se	<0.01	<0.01	Os	<0.01	<0.01
Br	<0.01	<0.01	Ir	<0.005	<0.005
Rb	<0.005	<0.005	Pt	<0.01	<0.01
Sr	<0.005	<0.005	Au	<0.05	<0.01
Y	<0.005	<0.001	Hg	<0.1	<0.1
Zr	<0.005	0.01	Tl	<0.005	<0.005
Mo	<0.01	3.3	Bi	<0.001	<0.001
Ru	<0.005	<0.005	Th	<0.00001	<0.0001
Rh	<0.005	<0.005	U	<0.00001	0.002

Table 2. Non-Metallic Impurity Content in Different Tungsten Samples

Element	CVD-UHPW/ppm	PM-W/ppm
C	<5	<5
N	<5	<5
O	<5	<5
H	<1	<1

The microstructures of the CVD-UHPW and PM-W samples, as observed by SEM and EBSD, are shown in Figure 4a−f. The CVD-UHPW exhibits a typical columnar-grained

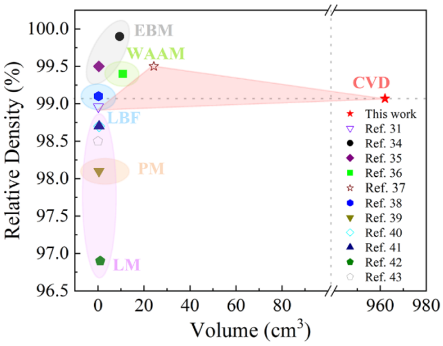

Figure 3. Density vs volume comparison of tungsten parts prepared by different methods.

microstructure (Figure 4a–f). The average grain size of the fine-grained layer is 5–20 μm, estimated using the cutoff method, while the coarse columnar grains range from 30–190 μm. In contrast, the PM-W shows a homogeneous microstructure of fine equiaxed grains with an average grain size of 20–200 μm (Figure 4g–i). Notably, numerous tiny holes are present within the equiaxed grains, indicating impurities introduced during the PM process. These observations suggest a complex interplay between residual impurities and microstructures in determining the ultimate densities and purities of different tungsten materials.

The TEM images of the two samples are shown in Figure 5. In both images, no precipitates or secondary phase particles are found. Dislocations are present within grains and at grain boundaries, with a higher density at the grain boundaries. However, the samples differ in dislocation distribution, dislocation density, phase interface morphology, and strain distribution. In PM-W, the dislocation distribution is uneven, with some areas showing a high density of tangled dislocations and dislocation walls (indicated by red arrows in Figure 5a). In contrast, CVD-UHPW has a more uniform dislocation distribution, with only a few regions exhibiting dislocation tangles.

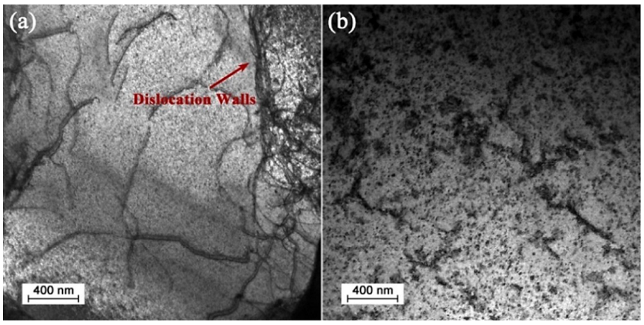

Figure 5. TEM images of (a) PM-W and (b) CVD-UHPW.

To further illustrate local features, the grain boundary morphologies of PM-W and CVD-UHPW are shown in Figure 6a–f. A higher density of dislocations is distributed along the grain boundaries in PM-W (Figure 6a) compared with that in CVD-UHPW (Figure 6d). High-resolution TEM images of the grain boundaries in PM-W (Figure 6b) and CVD-UHPW (Figure 6e) and their corresponding Fourier transform patterns reveal a high density of dislocations along the grain boundaries, with directions indicated in the corresponding

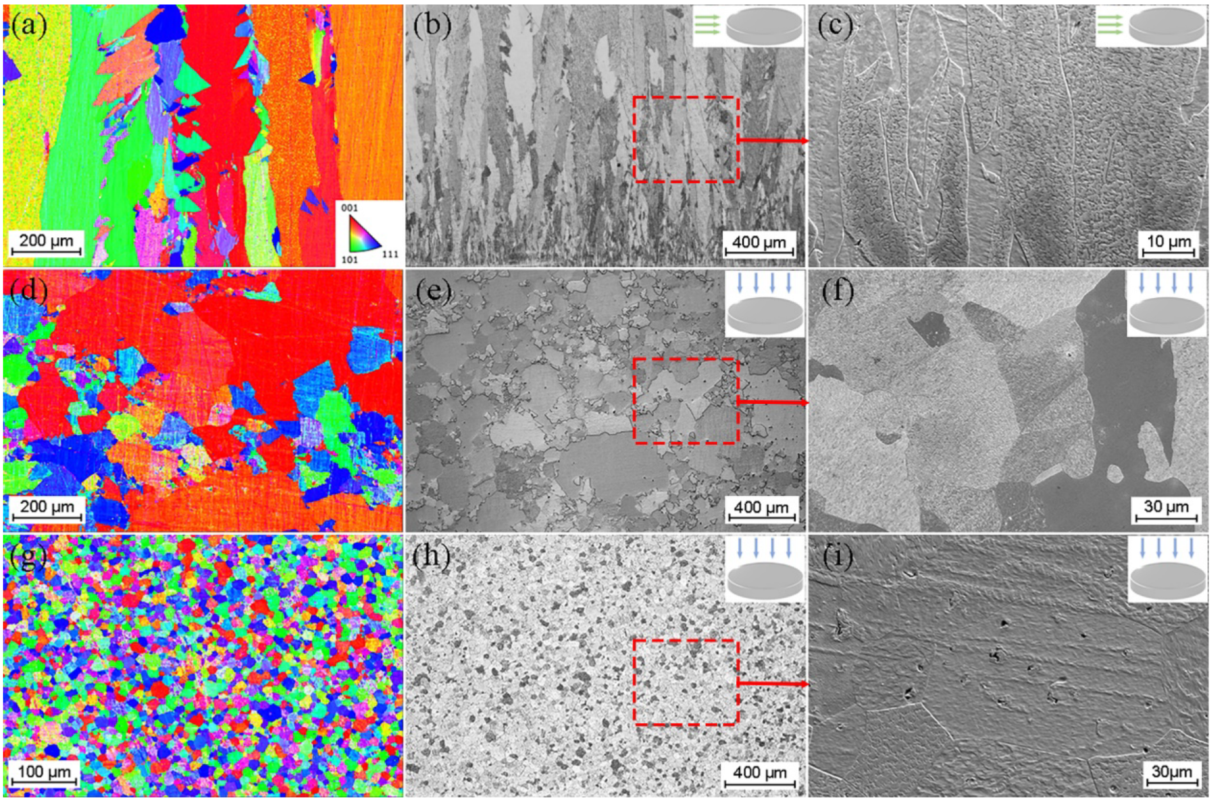

Figure 4. (a) EBSD IPF map and (b,c) SEM images (inset: the corresponding observation direction diagram) of CVD-UHPW from the side view. (d) EBSD IPF map and (e,f) SEM images (inset: the corresponding observation direction diagram) of CVD-UHPW from the top view. (g) EBSD IPF map and (h,i) SEM images (inset: the corresponding observation direction diagram) of PM-W from the top view.

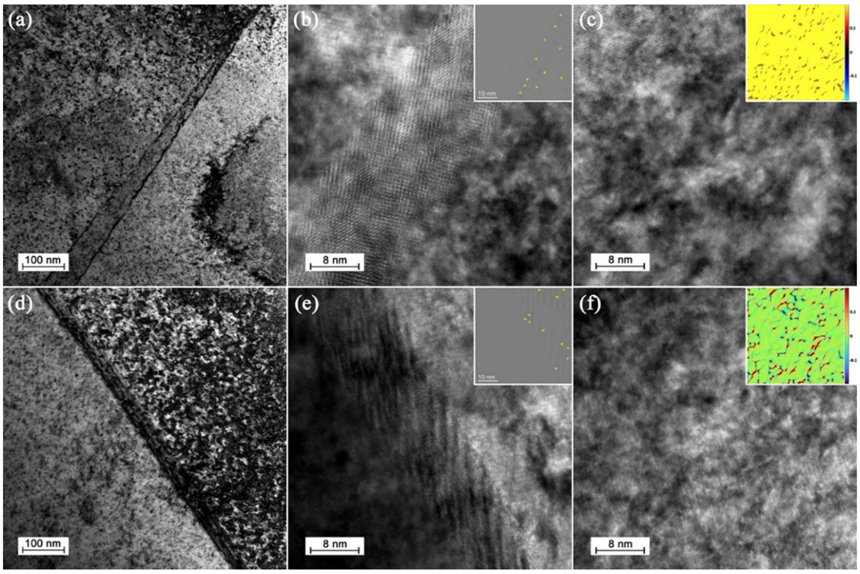

Figure 6. (a) TEM image of PM-W, (b) HRTEM image and Fourier transform patterns of the grain boundary for PM-W, and (c) TEM image and interior strain (inset) of the grain for PM-W. (d) TEM image of CVD-UHPW. (e) HRTEM image and Fourier transform patterns of the grain boundary for CVD-UHPW. (f) TEM image and interior strain (inset) of the grain for CVD-UHPW.

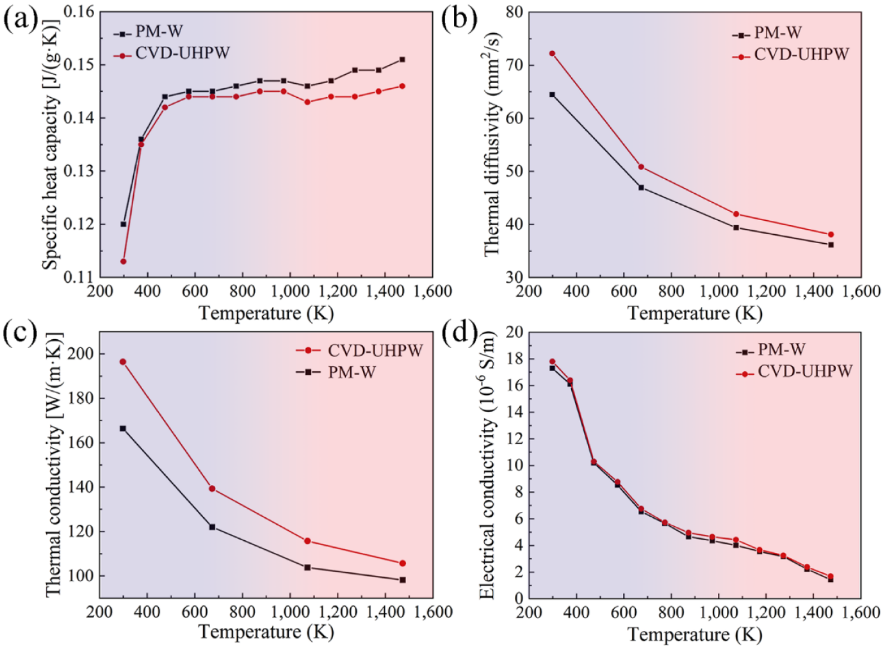

Figure 7. (a) Specific heat capacities, (b) thermal diffusivities, (c) thermal conductivities, and (d) electrical conductivities of CVD-UHPW and PM-W.

insets. The microstrain within grains (Figure 6c and f) reflects the uniformity of the material during the preparation process. Strain++ was used to analyze the grain interior strain in both PM-W and CVD-UHPW, as shown in the corresponding insets. The strain within the grains of PM-W is significantly higher than that in CVD-UHPW. These results are mainly due to numerous and evenly distributed nucleation centers formed by directional layer-by-layer deposition in the CVD method, which effectively impedes dislocation movement and reduce strain. The high uniformity of the CVD-UHPW metal microstructures implies that their use as sputtering targets will ensure increased sputtering yields and homogeneity of the resulting thin films.

Figure 7a−d shows the measured specific heat capacity, thermal diffusivity, thermal conductivity, and electrical conductivity, respectively, of the CVD-UHPW and PM-W samples over a temperature range from 298 to 1473 K. The following trends can be seen. First, the specific heat capacities of both samples increase with increasing temperature (Figure 7a), where the CVD-UHPW exhibits lower specific heat capacities at all testing temperatures. This lower specific heat capacity is attributed to the lower impurities of several specific metallic elements like Fe, Cr, and Ni, all of which possess a relatively higher theoretical heat capacity over W. Second, both thermal diffusivities and conductivities of CVD-UHPW and PM-W decrease with an increase in temperature (Figure 7b,c).

The values of CVD-UHPW are 5−8% higher than those of PM-W over the entire tested temperature range, due to the intensified electron scattering in the PM-W of higher impurities. Third, the electrical conductivities of CVD-UHPW and PM-W decrease with increasing temperature, while the measured values of the CVD-UHPW are 4% higher than those of the PM-W (Figure 7d). Overall, the CVD-UHPW exhibits a lower specific heat capacity, higher thermal diffusivity and conductivity, and higher electrical conductivity at the measuring temperature range, relative to the PM-W. These characteristics enable prolonged lifespan and enhance quality consistency when enduring extreme service conditions characterized by high particle fluxes and substantial heat loads.[44,45]

Finally, Figure 8 illustrates a typical actual application of the CVD-UHPW, in which the sputtering targets were made by machining from the CVD-UHPW plates described here. The square target measures 424 mm in length, 79 mm in width, and 4 mm in thickness, while the circular target has a diameter of 330 mm and a thickness of 7 mm. The feedback on the application from VLSI manufacturers confirms that the CVD-UHPW with enhanced physical properties exhibits superior performance. Furthermore, the present CVD method and the as-prepared CVD-UHPW parts could be adopted in other applications, e.g., the CVD-UHPW plates can be used directly to produce ultrafine particles (UFPs) without thermal shock-caused fractures,[29] and they can be mechanistically processed to form rods or wires used as the anode materials in high-performance short arc lamps.[46]

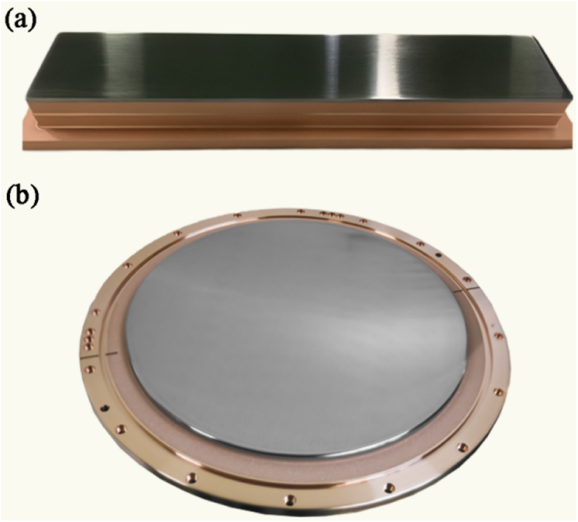

Figure 8. Schematic of (a) square and (b) round sputtering targets.

4. CONCLUSIONS

In summary, we successfully synthesized large-sized tungsten samples with an ultrahigh purity of up to 99.999998 wt % by the CVD method, utilizing ultrahigh purity WF_6 as the precursor. The resulting CVD-UHPW, characterized by coarse columnar grains, exhibits a high density close to the theoretical density, significantly higher than the PM-W counterpart with fine equiaxed grain microstructures. CVD-UHPW shows a lower density of dislocations along its grain boundaries and significantly reduced interior strain within its grains compared to PM-W. The specific heat capacity of CVD-UHPW is 3% lower than that of PM-W, while its thermal diffusivity and conductivity are increased by 5% and 8%, respectively. Electrical conductivity remains comparable across the temperature range from 298 K to 1473 K. These enhancements in physical properties are attributed to the lower impurities of other metallic and nonmetallic elements. These findings provide new insights into the design of next-generation UHPW materials with scalable sizes and significantly enhanced physical properties for semiconductor industrial applications.

■ ASSOCIATED CONTENT

Data Availability Statement

The raw/processed data required to reproduce these findings cannot be shared at this time, as the data also form part of an ongoing study.

■ AUTHOR INFORMATION

Corresponding Authors

Han Dong − *School of Materials Science and Engineering, Shanghai University, Shanghai 200444, China;* orcid.org/0000-0001-9117-0280; Email: mengxiangjun@tju.edu.cn

Xiangjun Meng − *PERIC Special Gas Co., Ltd, Handan City, Hebei Province 056000, China;* orcid.org/0009-0003-2897-1968; Email: qktgzsyx@163.com

Authors

Lipei Peng − *School of Materials Science and Engineering, Shanghai University, Shanghai 200444, China; PERIC Special Gas Co., Ltd, Handan City, Hebei Province 056000, China*

Shiwei Wu − *Department of Mechanical Engineering, National University of Singapore, Singapore 117575, Singapore*

Xicheng Wei − *School of Materials Science and Engineering, Shanghai University, Shanghai 200444, China*

Wei Peng − *School of Materials Science and Engineering, Shanghai University, Shanghai 200444, China*

Yafeng Wang − *PERIC Special Gas Co., Ltd, Handan City, Hebei Province 056000, China*

Tengshi Liu − *School of Materials Science and Engineering, Shanghai University, Shanghai 200444, China*

Shaobo Li − *PERIC Special Gas Co., Ltd, Handan City, Hebei Province 056000, China*

Complete contact information is available at:
https://pubs.acs.org/10.1021/acsomega.4c06723

Author Contributions

L.P. conceived the idea, collected the data, and wrote the draft; Y.W. and T. L. collected the data; X.M., H.D., S.L., X.W., W.P., and S.W. contributed to conceiving the idea of the study. All authors contributed to the writing and revisions.

Notes

The authors declare no competing financial interest.

■ ACKNOWLEDGMENTS

This study was financially supported by PERIC Special Gas Co., Ltd. by supplying the equipment and materials.

■ REFERENCES

(1) Pirker, L.; Višić, B. Recent progress in the synthesis and potential applications of two-dimensional tungsten (sub) oxides. *Isr. J. Chem.* **2022**, *62* (3−4), No. e202100074.

(2) Zhang, H.; Zhang, H.-W.; Qiao, L.; Zhang, X.-X.; He, R.; Wang, P. Erosion and deuterium retention behavior of tungsten exposed to impurity-seeded deuterium plasma. *Tungsten* **2021**, *3* (4), 448−458.

(3) Terentyev, D.; Chang, C. C.; Yin, C.; Zinovev, A.; He, X. F. Neutron irradiation effects on mechanical properties of ITER specification tungsten. *Tungsten* **2021**, *3* (4), 415−433.

(4) Xu, H.; He, L. L.; Pei, Y. F.; Jiang, C. Z.; Li, W. Q.; Xiao, X. H. Recent progress of radiation response in nanostructured tungsten for nuclear application. *Tungsten* **2021**, *3*, 20−37.

(5) Jiang, Y.; Huang, P.; Jiang, Z. Q.; Hou, J.; Xu, Z.; Wu, E. H.; Li, J. Gradient nanostructured tungsten and the thermal shock response. *Tungsten* **2023**, *5* (4), 548−557.

(6) Candela-Juan, C.; Niatsetski, Y.; Van Der Laarse, R.; Granero, D.; Ballester, F.; Perez-Calatayud, J.; Vijande, J. Design and characterization of a new high-dose-rate brachytherapy Valencia applicator for larger skin lesions. *Med. Phys.* **2016**, *43* (4), 1639−1648.

(7) Liu, T. L.; Kim, C. J. Turning a surface superrepellent even to completely wetting liquids. *Science* **2014**, *346* (6213), 1096−1100.

(8) Olsson, M.; Bushlya, V.; Lenrick, F.; Ståhl, J.-E. Evaluation of tool wear mechanisms and tool performance in machining single-phase tungsten. *Int. J. Refract. Met. Hard Mater.* **2021**, *94*, 105379.

(9) Chen, Z.; Han, W.; Yu, J.; Kecskes, L.; Zhu, K.; Wei, Q. Microstructure and helium irradiation performance of high purity tungsten processed by cold rolling. *J. Nucl. Mater.* **2016**, *479*, 418−425.

(10) Lo, C. F.; McDonald, P.; Draper, D.; Gilman, P. Influence of tungsten sputtering target density on physical vapor deposition thin film properties. *J. Electron. Mater.* **2005**, *34*, 1468−1473.

(11) Xu, Z.; Bai, J.; Qian, L. Surface microstructural alterations and grain refinement mechanisms of tungsten heavy alloys by thermo-mechanical coupling: A laser-assisted milling case. *J. Manuf. Process* **2023**, *108* (22), 359−372.

(12) Zhan, J.; Wang, H.; Wang, H.; Li, M.; He, J.; Zhu, J.; Zhao, B. Preparation of high-density and excellent bending strength pure tungsten target by hot oscillatory pressing sintering and its magnetron sputtering coating. *Int. J. Refract. Met. Hard Mater.* **2024**, *123*, 106773.

(13) Cui, W.; Flinders, K.; Hancock, D.; Grant, P. S. Joining and cycling performance of ultra-thick tungsten coatings on patterned steel substrates for fusion armour applications. *Mater. Design* **2021**, *212*, 110250.

(14) Bakke, J.; Lei, Y.; Xu, Y. Fluorine-free tungsten films as low resistance liners for tungsten fill applications. *2016 IEEE International Interconnect Technology Conference/Advanced Metallization Conference, (IITC/AMC)*; IEEE, 2016; pp. 108110.

(15) Lassner, E.; Schuber, W. D. *Properties, chemistry, technology of the element, alloys, and chemical compounds*; Kluwer Academic/Plenum Publishers: New York, 1999.

(16) Liu, W.; Long, L.; Ma, Y. Research and preparation methods for high-purity tungsten. *Powder Metal. Technol.* **2012**, *30* (3), 223−228.

(17) Liu, W.; Long, L.; Ma, Y.; Cai, Q. Research of process and principle of debinding of powder extrusion-molded compacts. *Powder Metal. Technol.* **2011**, *29* (1), 54−61.

(18) Chen, Y. L.; Guo, X. Y.; Wang, Q. M.; Tian, Q. H.; Huang, S. B.; Zhang, J. X. Tungsten and arsenic substance flow analysis of a hydrometallurgical process for tungsten extracting from wolframite. *Tungsten* **2021**, *3* (3), 348−360.

(19) Ma, J.; Liu, W.; Wang, C.; Chang, J. H. The effect of CVD temperature on the micro-structure and properties of tungsten deposition layers (in Chinese). *China Surf. Eng.* **2008**, *21* (5), 21−25.

(20) Ma, J.; Wei, J.; Wang, C.; et al. Effect of temperature on the structure and surface morphology of tungsten in chemical vapor deposition. *China Surf. Eng.* **2020**, *23* (1), 30−33.

(21) Ma, J.; Wei, J.; Wang, C.; Fan, A. Study on the performance of tungsten tube prepared by chemical vapor deposition method. *Acta Armamentarii* **2011**, *32* (6), 703−706.

(22) Jie, M.; Hao-dong, Z.; An-yuan, B.; Cong-zeng, W.; Mei-Iing, Z. Study on the preparation of irregular tungsten products by chemical vapor deposition. *Acta Armamentarii* **2006**, *27* (2), 315−319.

(23) Lai, K. K.; Lamb, H. H. Tungsten chemical vapor deposition using tungsten hexacarbonyl: microstructure of as-deposited and annealed films. *Thin Solid Films* **2000**, *370* (1−2), 114−121.

(24) Tamura, S.; Tokunaga, K.; Yoshid, N. High heat load properties of high purity CVD tungsten. *J. Nucl. Mater.* **2002**, *307*, 735−738.

(25) Piazza, G.; Matthews, G. F.; Pamela, J.; Altmann, H.; Coad, J. P.; Hirai, T.; Lioure, A.; Maier, H.; Mertens, P. H.; Philipps, V.; et al. R&D on tungsten plasma facing components for the JET ITER-like wall project. *J. Nucl. Mater.* **2007**, *367*, 1438−1443.

(26) Matejícek, J.; Chráska, P.; Linke, J. Thermal spray coatings for fusion applications. *Therm. J. Spray Technol.* **2007**, *16*, 64−83.

(27) Pintsuk, G.; Smid, I.; Döring, J.; Hohenauer, W.; Linke, J. Fabrication and characterization of vacuum plasma sprayed W/Cu-composites for extreme thermal conditions. *J. Mater. Sci.* **2007**, *42*, 30−39.

(28) Hirai, T.; Kreter, A.; Linke, J.; Malzbender, J.; Ohgo, T.; Philipps, V.; Pintsuk, G.; Pospieszczyk, A.; Sakawa, Y.; Sergienko, G.; Tanabe, T.; Ueda, Y.; Wada, M. Critical heat flux loading experiments on CVD-W coating in the TEXTOR tokamak. *Fus. Eng. Des.* **2006**, *81*, 175−180.

(29) Kim, P.; Mihara, Y.; Ozawa, E.; Nozawa, Y.; Hayashi, C. High purity metal production using dry refining processes. *Mater. Trans., JIM* **2000**, *41* (1), 37−43.

(30) Lv, Y. Research on crystal growth habits and application properties of chemical vapor deposition tungsten material (in Chinese). *Rare Metal Mater. Eng.* **2017**, *46* (9), 2499−2504.

(31) Lv, Y.; Song, J.; Lian, Y.; Yu, Y.; Liu, X.; Zhuang, Z. The thermal properties of high purity and fully dense tungsten produced by chemical vapor deposition. *J. Nucl. Mater.* **2015**, *457*, 317−323.

(32) Peng, L.; Dong, H.; Li, S.; Wang, Z.; Meng, X.; Wang, Y.; Liu, T.; Li, X.; Ji, J. Numerical simulation study on flow and heat transfer of the tungsten crucible CVD reactor. *ACS Omega* **2022**, *7* (46), 42044−42055.

(33) Wei, X. Preparation technology and application of high purity tungsten target materials (in Chinese). *Hard Alloy* **2017**, *34* (5), 353−359.

(34) Dorow-Gerspach, D.; Kirchner, A.; Loewenhoff, T.; Pintsuk, G.; Weißgärber, T.; Wirtz, M. Additive manufacturing of high density pure tungsten by electron beam melting. *Nucl. Mater. Energy* **2021**, *28*, 101046.

(35) Yang, G.; Yang, P.; Yang, K.; Liu, N.; Jia, L.; Wang, J.; Tang, H. Effect of processing parameters on the density, microstructure and strength of pure tungsten fabricated by selective electron beam melting. *Int. J. Refract. Hard Met* **2019**, *84*, 105040.

(36) Marinelli, G.; Martina, F.; Lewtas, H.; Hancock, D.; Mehraban, S.; Lavery, N.; Ganguly, S.; Williams, S. Microstructure and thermal properties of unalloyed tungsten deposited by wire + arc additive manufacture. *J. Nucl. Mater.* **2019**, *522*, 45−53.

(37) Chen, Z.; Lian, Y. Y.; Liu, X.; Feng, F.; Yan, B. Y.; Wang, J. B.; Lv, Y. W.; Song, J. P.; Liu, C. J.; Cai, L. Z. Recent research and development of thick CVD tungsten coatings for fusion application. *Tungsten* **2020**, *2*, 83−93.

(38) Todo, T.; Ishimoto, T.; Gokcekaya, O.; Oh, J.; Nakano, T. Single crystalline-like crystallographic texture formation of pure tungsten through laser powder bed fusion. *Scr. Mater.* **2022**, *206*, 114252.

(39) Zhang, X.; Yan, Q.; Lang, S.; Xia, M.; Ge, C. Thermal shock performance of sintered pure tungsten with various grain sizes under transient high heat flux test. *J. Fusion Energy* **2016**, *35* (4), 666−672.

(40) Wen, S.; Wang, C.; Zhou, Y.; Duan, L.; Wei, Q.; Yang, S.; Shi, Y. High-density tungsten fabricated by selective laser melting: densification, microstructure, mechanical and thermal performance. *Opt Laser Technol.* **2019**, *116*, 128−138.

(41) Wang, D.; Yu, C.; Zhou, X.; Ma, J.; Liu, W.; Shen, Z. J. Dense pure tungsten fabricated by selective laser melting. *Appl. Sci.* **2017**, *7* (4), 430.

(42) Zi, X.; Chen, C.; Wang, X.; Wang, P.; Zhang, X.; Zhou, K. Spheroidisation of tungsten powder by radio frequency plasma for selective laser melting. *Mater. Sci. Technol.* **2018**, *34* (6), 735−742.

(43) Tan, C.; Zhou, K.; Ma, W.; Attard, B.; Zhang, P.; Kuang, T. Selective laser melting of high-performance pure tungsten: parameter design, densification behavior and mechanical properties. *Sci. Technol. Adv. Mater.* **2018**, *19* (1), 370−380.

(44) Yin, H.; Cheng, L.; Zhang, X.; Zhang, H.; Guo, W.; Yuan, Y.; Yan, B.; Wang, P.; Lu, G. H. Surface blistering and deuterium retention in chemical vapor deposition tungsten exposed to deuterium plasma. *Nucl. Mater. Energy* **2023**, *37*, 101536.

(45) Yi, X. O.; Kuwabara, T.; Alimov, V. K.; Du, Y. F.; Han, W. T.; Liu, P. P.; Yan, B. Y.; Song, P. J.; Yoshida, K.; Toyama, T.; Wan, F. R.; Ohnuki, S.; Hatano, Y.; Nagai, Y. Microstructure, hardening and deuterium retention in CVD tungsten irradiated with neutrons at temperatures of defect recovery stages II and III. *Tungsten* **2022**, *4* (3), 248−260.

(46) Yu, Y.; Song, J.; Bai, F.; Zheng, A.; Peng, F. Ultra-high purity tungsten and its applications. *Int. J. Refract. Met. Hard Mater.* **2015**, *53*, 98−103.